Fast Radial Symmetry Detection Under Affine Transformations

Jie Ni*
jni@umiacs.umd.edu
Center for Automation Research
Univ. of Maryland, College Park, MD 20742

Maneesh K. Singh and Claus Bahlmann
{maneesh.singh, claus.bahlmann}@siemens.com
Siemens Corporate Research and Technology
Siemens Co., Princeton, NJ 08540

Abstract

The fast radial symmetry (FRS) transform has been very popular for detecting interest points based on local radial symmetry [1]*. Although FRS delivers good performance at a relatively low computational cost and is very well suited for a variety of real-time computer vision applications, it is not invariant to perspective distortions. Moreover, even perfectly (radially) symmetric visual patterns in the real world are perceived by us after a perspective projection. In this paper, we propose a systematic extension to the FRS transform to make it invariant to* (bounded) cases *of perspective projection - we call this transform the generalized FRS or GFRS transform. We show that GFRS inherits the basic characteristics of FRS and retains its computational efficiency. We demonstrate the wide applicability of GFRS by applying it to a variety of natural images to detect radially symmetric patterns that have undergone significant perspective distortions. Subsequently, we build a nucleus detector based on the GFRS transform and apply it to the important problem of digital histopathology. We demonstrate superior performance over state-of-the-art nuclei detection algorithms, validated using ROC curves.*

1. Introduction

Symmetry of all kinds, including the visual, is ubiquitous in our world. Indeed, visual symmetry can be copiously seen in nature as well as in human creations: buildings, objects, our works of art. Perception of visual symmetry is thought to play an important biological and evolutionary role in humans as well in other species (for examples, see [2],[3]). Perhaps due to this importance of visual symmetry, humans seem to be able to recover symmetry in shapes and random textures within 100ms [4].

This paper deals with symmetry of the radial kind. Our world abounds in objects and structures that are (partially) radially symmetric - natural objects including the heavenly bodies, several fruits and vegetables, human heads, textured patterns like the spots on a cheetah, a variety of man-made objects including balls, coins, wheels, tapes, manholes, circular tabletops, ends of cylindrical objects as well as innumerable examples from works of art. Accordingly, computation of radial symmetry has attracted due interest from the computer vision community (e.g. [5], [1], [6]). For an excellent recent exposition, refer to [7].

However, the issue of perspective projection in fast radial symmetry detection seems to have received lesser attention - one work in this direction is [8]. Humans perceive objects after a perspective projection. It is well known that under (bounded cases) of perspective projection, circles give rise to ellipses. Thus, (roughly) radially symmetric visual patterns would be perceived as elliptical by our eyes. To be able to handle perspective projections, it is very important that radial symmetry detectors principally incorporate detection of elliptical radial symmetry in visual patterns.

We are interested in fast computation of radial symmetries. The best run-time [7] is achieved by the Fast Radial Symmetry (FRS) transform proposed by Loy and Zelinsky [1] in 2003. FRS uses a Hough Transform [9] like voting scheme to detect points of local radial symmetry. However, instead of using a 3-dimensional parameter space for voting, it estimates

*Work performed at Siemens Corporate Research.

[1]The term radial symmetry is used in the sense of circular symmetry, as in the FRS paper [1].

the local differential properties of the image to reduce the voting space to be 1-dimensional (scale/ radii axis). For detecting circles of a give size, the algorithm is O(N) where N is the number of image pixels.

We make the following contributions in this paper: (1) We systematically extend the FRS transform to incorporate detection of elliptical symmetry while leveraging the very good complexity behavior of the FRS algorithm. We extend the idea of using local differential structure of images (in FRS) to make it work for a class of affine spatial transformations. The proposed algorithm is parametrized to be able to use FRS as a module and thus retains its attractive features like simplicity and fast computational speed. We call the proposed method - the Generalized Fast Radial Symmetry (GFRS) transform. (2) We demonstrate the wide applicability of GFRS by applying it to a variety of natural images to detect radially symmetric patterns that have undergone significant perspective distortions. (3) Finally, we quantitatively validate the novel GFRS transform by applying it to the problem of (cell) nuclei detection in histopathology slides - these nuclei are elliptical in nature. For this purpose, we train a simple nucleus detector based on the GFRS transform and show superior performance over state-of-the-art nuclei detection algorithms (including one based on the FRS detector). We validate the performance through quantitative measurement of precision and recall.

The rest of the paper is structured as follows: In subsection 1.1, we place this work in context with the state of art in computer vision. In Section 2, we present the Generalized Fast Radial Symmetry (GFRS) transform. We present experimental results on natural images in subsection 3.1, and subsequently, in subsection 3.2, we present the application of the ellipse detector based on the GFRS transform to nuclei detection. We summarize the contributions of the paper in Section 4.

1.1. Related Work

An area related to our work is that of affine invariant interest point detectors or (local) feature detectors - for an excellent survey, see [10]. Affine invariant detectors like Harris-Affine and Hessian-Affine are local in nature though they do respond to blob-like features as well. These detectors only use the very local differential properties of the image. GFRS uses the local differential image properties but agglomerates them using an underlying elliptical model. Even though many of these invariant detectors analyze local second order image properties and output elliptical representations, these are based on a fitting process and not on detection of radial symmetry. Similar is the case with region detectors like MSER [11].

More closely related is ellipse detection using Generalized Hough Transforms (GHT) [9]. However, this requires dense sampling in the 5-dimensional parameter space (c_x, c_y, θ, a, b) - which can be computationally prohibiting. Indeed, to alleviate this problem, Loy and Zelinski [1] proposed the Fast Radial Symmetry (FRS) based on an efficient voting algorithm. It transforms an input image to a transform image which highlights points of high radial symmetry. The algorithm is very efficient with a complexity linear in the size of the image (for each scale). However, it is not invariant to perspective distortions. Our work addresses precisely this issue. We systematically extend the FRS algorithm to detect radial symmetries while being invariant to perspective transformations.

More recently, Cornelius and Loy [8] proposed an approach to detect radial symmetry under affine projections. However, their approach is computationally intensive: affine invariant features are detected and SIFT descriptors are computed for matching. Subsequently, all pairs of matched features are used to vote for ellipse hypotheses. We, on the other hand, provide a natural extension to the FRS transform retaining the computational efficiency of the original algorithm.

2. Generalized Fast Radial Symmetry (GFRS) Transform

2.1. Fast radial symmetry transform

We summarize here the fast radial symmetry transform method. Interested readers may refer to [1] for more details. For each radius n, the algorithm uses image gradients to vote for both the positively-affected and negatively-affected pixels which are defined as

$$\mathbf{p}_{+ve}(\mathbf{p}) = \mathbf{p} + \text{round}\left(\frac{\mathbf{g}(\mathbf{p})}{||\mathbf{g}(\mathbf{p})||}n\right) \quad (1)$$

$$\mathbf{p}_{-ve}(\mathbf{p}) = \mathbf{p} - \text{round}\left(\frac{\mathbf{g}(\mathbf{p})}{||\mathbf{g}(\mathbf{p})||}n\right) \quad (2)$$

$\mathbf{p}_{+ve}(\mathbf{p}), \mathbf{p}_{-ve}(\mathbf{p})$ correspond to pixels with the gradient $\mathbf{g}(\mathbf{p})$ pointing towards and away from the center

respectively. From those pixels, an orientation projection image O_n and a magnitude projection image M_n are formed. Specifically, for each positively affected pixel, the corresponding point $\mathbf{p}_{+ve}$ in $\mathbf{O}_n$ and $\mathbf{M}_n$ is increased by 1 and $||\mathbf{g}(\mathbf{p})||$, respectively. Similarly, for the negatively affected pixel, the corresponding point is decreased by the same quantity in each image.

The radial symmetry response map is defined as

$$S_n = F_n * A_n \tag{3}$$

where

$$F_n(\mathbf{p}) = \frac{M_n(\mathbf{p})}{k_n}\left(\frac{|\tilde{O}_n(\mathbf{p})|}{k_n}\right)^{\alpha} \tag{4}$$

$$\tilde{O}_n(\mathbf{p}) = \begin{cases} O_n(\mathbf{p}), & O_n(\mathbf{p}) < k_n \\ k_n, & otherwise \end{cases} \tag{5}$$

A_n is an isotropic Gaussian smoothing function, α is the radial strictness parameter, and k_n is a scaling factor across different radii.

While [1] is very effective at detecting locii of circular radial symmetry, FRS is not invariant to spatial transformations arising due to perspective projections. In such cases the gradient direction deviates from the radial vector, which leads to diffusion and dispersion of the locus of symmetry in the object space [12]. In the case of bounded perspective projection, it is well known that circular structures project as elliptical structures. Thus, to handle geometric distortions due to perspective projections, there is a need to extend FRS to handle elliptical symmetries. We use here a simple observation from geometry: an ellipse can be represented as an affine transform of a unit circle. Utilizing this affine relationship, we propose to get a modified voting procedure to generalize the FRS algorithm to render it invariant to (bounded) perspective transformations. We describe the details below.

2.2. Generalized radial symmetry voting

Let $p(\phi)$ be the parametrization of a circle

$$p(\phi) = (\cos(\phi) + c_x, \sin(\phi) + c_y)^T, 0 \leq \phi < 2\pi \tag{6}$$

where $c = (c_x, c_y)^T$ is the center of the circle. Then, the ellipse $q(\phi)$ centered at c, with orientation θ and semi-major and semi-minor axes (a, b) respectively, can be obtained by a suitable affine transformation $G \in A(2)$,

$$q(\phi) = G \cdot (p(\phi) - c) + c,\ G = R \cdot S \tag{7}$$

$$R = \begin{pmatrix} \cos(\theta) & -\sin(\theta) \\ \sin(\theta) & \cos(\theta) \end{pmatrix}, S = \begin{pmatrix} a & 0 \\ 0 & b \end{pmatrix},$$

where R, S are the rotation and scaling matrix respectively. We denote $A(2)$ as the group of affine transformation of the plane [13], and we restrict G to be a member of $A(2)$ to ensure the uniqueness of the affine transformation [14].

Let the corresponding tangent and normal vectors at $p(\phi)$ and $q(\phi)$ be $T_{p(\phi)}, T_{q(\phi)}$ and $N_{p(\phi)}$, $N_{q(\phi)}$ respectively. We derive two propositions following from the simple fact that since $G : R^2 \rightarrow R^2$ is a linear transform, the relevant tangent and normal subspaces are also related by the same transformation G.

Proposition 1. *The tangent vector $T_{q(\phi)}$ at the point $q(\phi)$ on the ellipse can be obtained through the affine transform G of the tangent vector $T_{p(\phi)}$ at the corresponding point $p(\phi)$ on the circle, i.e., $T_{q(\phi)} = G \cdot T_{p(\phi)}$.*

Proof. Follows from differentiating (7): $T_{q(\phi)} = \partial_\phi q(\phi) = \partial_\phi G \cdot p(\phi) = G \cdot T_{p(\phi)}$ □

Proposition 2. *The voting vector $V_{q(\phi)}$ toward the centroid of the ellipse at point $q(\phi)$ can be obtained through the affine transform G of the normal vector $N_{p(\phi)}$ of the corresponding point $p(\phi)$ on the circle, i.e., $V_{q(\phi)} = G \cdot N_{p(\phi)}$.*

Proof. Since $V_{q(\phi)} = c - q(\phi)$ and $N_{p(\phi)} = c - p(\phi)$, the result follows from (7). □

This leads to the main result of our paper.

Proposition 3. *Let $\hat{T}_{q(\phi)}$ be an unbiased estimator of the tangent at $q(\phi)$. Then, the unbiased estimator of the voting direction is given by*

$$\hat{V}_{q(\phi)} = G \cdot M \cdot G^{-1} \cdot \hat{T}_{q(\phi)} \tag{8}$$

where $M = \begin{bmatrix} 0 & 1 \\ -1 & 0 \end{bmatrix}$.

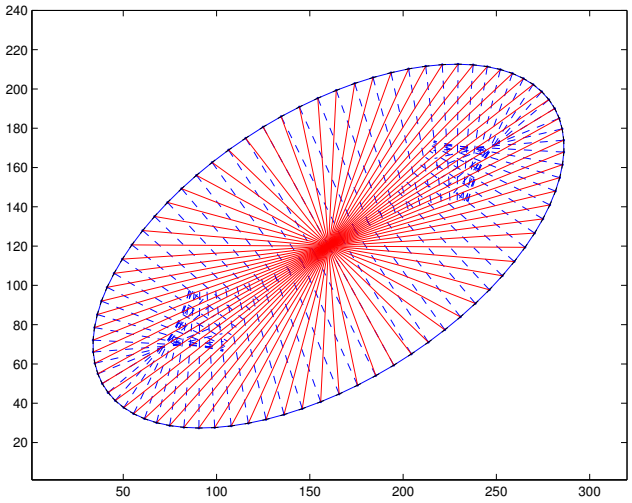

Figure 1. Voting direction $V_{q(\phi)}$ for the ellipse's centroid (in red) vs. Original normal vectors $N_{q(\phi)}$ on the ellipse (in blue).

Proof. $V_{q(\phi)} = G \cdot N_{p(\phi)} = G \cdot M \cdot T_{p(\phi)} = G \cdot M \cdot G^{-1} \cdot T_{q(\phi)}$.

The first equality follows from Proposition 2, the second from the fact that M relates the tangent and normal spaces and the third from Proposition 1. □

In Figure 1, we illustrate that the voting vectors $\hat{V}_{q(\phi)}$ (red lines), as computed by (8) have the correct directions as they all correctly intersect at the center of the ellipse. On the other hand, the voting directions of FRS, aligned with the normal to the curve, are incorrect. These are depicted as dashed blue lines.

Consequently, for a given G, we can use local differential image characteristics to vote for the ellipses of that particular shape. Therefore, for a point sampled from the constrained affine group $A(2)$, we transform the image gradient voting vector $\mathbf{g}(\mathbf{p})$ via

$$\hat{V}_{q(\phi)} = G \cdot M \cdot G^{-1} \cdot M^{-1} \cdot \mathbf{g}(\mathbf{p}) \tag{9}$$

and modify the voting scheme as described by Eqs (1) and (2) using the new voting directions:

$$\mathbf{p}_{+ve}(\mathbf{p}) = \mathbf{p} + \text{round}\left(\frac{\hat{V}_{q(\phi)}}{||\hat{V}_{q(\phi)}||} n\right) \tag{10}$$

$$\mathbf{p}_{-ve}(\mathbf{p}) = \mathbf{p} - \text{round}\left(\frac{\hat{V}_{q(\phi)}}{||\hat{V}_{q(\phi)}||} n\right) \tag{11}$$

Then, each value of G provides us with a response map, which captures evidence for ellipses of that particular size, shape, and orientation. Note that G induces a natural parametrization for the space of ellipses and a consequent generalization of the FRS algorithm (GFRS). We can now span the desired range of the 3D parameter space of $A(2)$, compute the GFRS map for each parameter and use the resultant stack of response maps as an interest point map for ellipses of all desired sizes, shapes and orientations. The final response map is obtained through maximization at each pixel location among all the response maps.

We now consider two practical aspects.

Normalizing factor k_n: As the length of the major/minor axis of ellipse changes, so does the number of gradient votes from the perimeter of the ellipse. To alleviate this bias, we follow the suggestion in [1], and empirically determine the normalizing factor k_n (see 4) for ellipse across different affine transformation parameters a and b.

Smoothing: We modified the smoothing performed in (3) to be consistent with the chosen affine transformation. This is motivated by the observation that, under noise, the deviation of the voting location from the true center is proportional to the length of $V_{q(\phi)}$. Thus, we choose a 2d Gaussian blurring kernel, specified by affine transform parameters θ, a, and b.

3. Experimental Validation

In previous sections, we extended the computationally-efficient FRS algorithm to get affine invariance. We now experimentally validate this contribution: we apply the GFRS transform for radial symmetry detection in a variety of real world images as well as for nuclei detection in histopathological images.

3.1. Real world images

In the introduction, we argued that our world abounds in radially symmetric objects and their (perspectively projected) images. Since there are no standard ellipse detection benchmark datasets, we selected a variety of everyday images to demonstrate the breadth of applicability of GFRS and to qualitatively compare the results with the baseline FRS. The examples we present contain wheels from different kinds of vehicles, as well as other objects like tomatoes and

coins. In Figure 2, we show the response map from GFRS in the top row and the corresponding image overlaid with detections in the bottom row. We observe that the GFRS response maps capture locations of radially symmetric structures very effectively, despite perspective transformations and other challenging conditions, e.g, cluttered background, partial occlusion of objects' elliptical-arcs, lack of contrast in regions of interest etc. The high response regions coincide well with locations of radially symmetric objects like wheels, coins etc. Note that the range of scales of the sampling points from $A(2)$ is chosen to not target very small objects to avoid cluttering the qualitative results. We observe that the overlaid ellipses also coincide well with the boundaries of the radially symmetric objects. This shows that GFRS is also able to estimate the affine parameters quite accurately.

For comparison, we applied FRS to some images of Figure 2. The results are shown in Figure 3. As expected, GFRS is able to detect radial symmetry in the presence of significant perspective distortions while FRS doesn't do quite as well in these scenarios.

3.2. Nuclei detection

We now access the performance of GFRS for detecting nuclei in biopsy samples from histopathological images. Nuclei detection is a fundamental step in the automatic prognosis of breast cancer. Different methods have been proposed in the literature, for e.g., a linear SVM approach [15], a Hessian matrix based approach [16], a circular Hough transform based approach [17] etc. In this paper, though, we exploit the a-priori knowledge that nuclei are usually elliptical in shape, and apply the GFRS transform to extract those elliptical regions of interest. Sampling of the 3d affine transformation space is done by the following parameter values: a=[6, 8, 10, 12, 14, 16], b=[4, 6, 8], θ = [i*π/8,i=0,1,...,7]. Then from the output response map, we retain as interest points all non-maximally suppressed locations above a certain threshold value. Each interest point is associated with a confidence value and an elliptical region which is described by five ellipse parameters.

We carried out experiments on nuclei detection using 512×512 image patches that were taken from large (several GPixel) H&E stained "virtual slides". These slides were sampled at 0.47 microns/pixel, corresponding to 40X objective scan. Figure 4 shows the nuclei detection results from a typical histopathological image. We show the response map on the left, and the extracted nuclei on the right. We plot ellipses on top of the detected nuclei, and the color of the ellipses represents the confidence value. We observe that GFRS can effectively detect nuclei with various shapes, even in challenging cases of touching/overlapping nuclei. In addition to identifying the nuclei centers, GFRS provides additional information about the size and orientation of the nuclei from the extracted elliptical region. This side information can be used to facilitate follow-up processing and analysis for segmentation, linking, and detection of other conditions like malignancy.

We also carried out quantitative evaluation and comparison of the GFRS based nuclei detector. For this purpose, we constructed a ground truth dataset by manually annotating all nuclei centroids from five images of size 512×512 — in all, 2555 nuclei were annotated.

We then applied GFRS and evaluated its performance using precision-recall curves. We compared our results with those from related state of the art - radial symmetry transform [1], Hessian matrix based detection [16], SVM based detection [15]. We plot the precision and recall curves in Figure 5. GFRS clearly achieves the best performance among all the algorithms that were tested on this problem. For example, for a recall of 95%, only every 13th detection corresponds to a false alarm. None of the other approaches achieves comparable performance.

3.3. Computational complexity

In our experiments, it takes around 20ms for each sampled affine transform, G_i, to generate a response map for a 375x250 image (~16ms for FRS). The number of parameters sampled from 3d affine space for each image varies from 50 to 200. However, with application-specific priors, e.g., rough knowledge of camera height and viewing angle in a surveillance/traffic-like static camera setting, GFRS reduces to almost the same sampling set size as FRS (1d scale space). Since GFRS is highly parallelizable (as is FRS), multicore-CPU/ GPU targeted implementations can make the algorithm practically real-time.

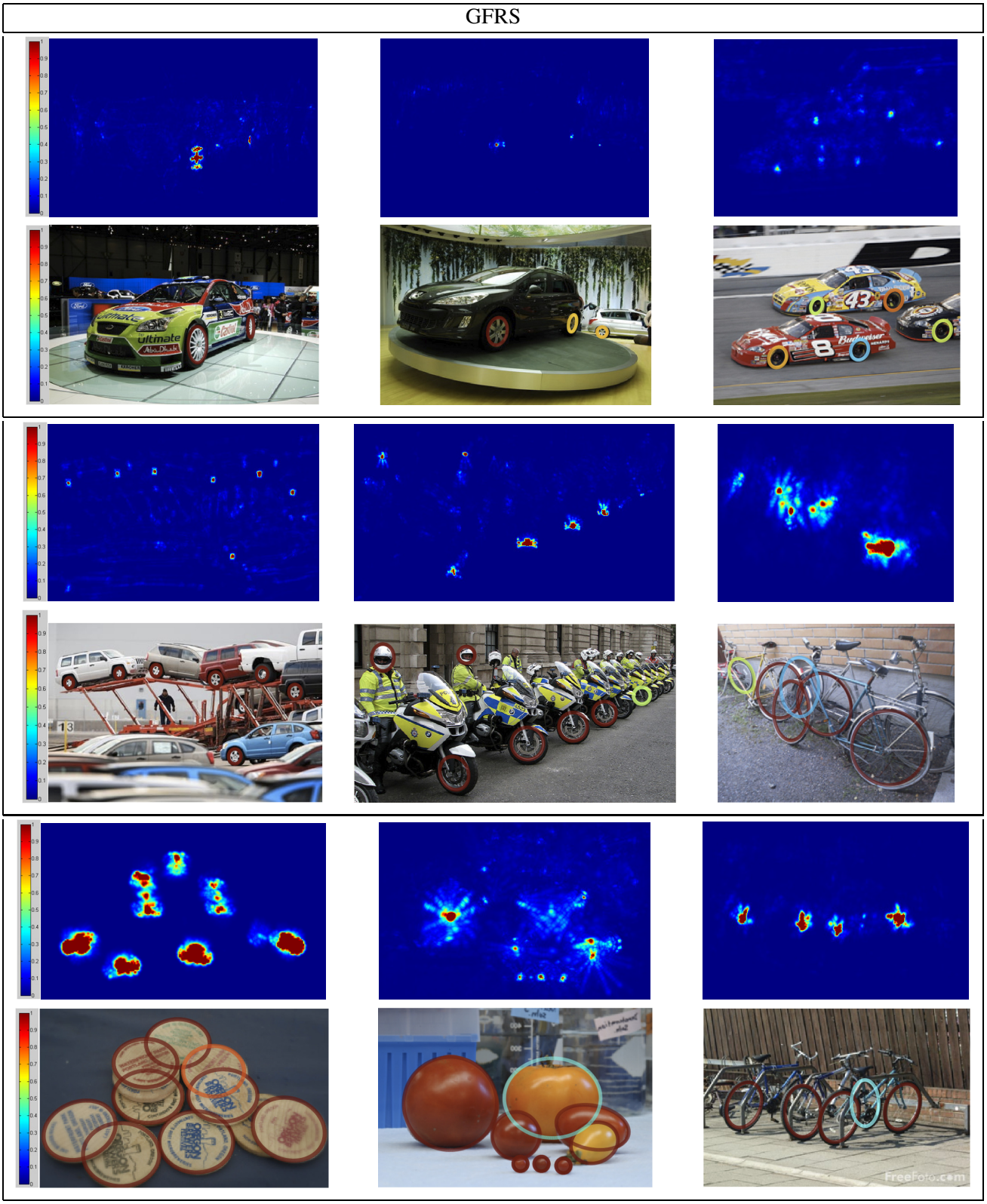

Figure 2. GFRS applied to real world images. Each pair of images shows the GFRS response map and the most confident detections corresponding to ellipses after thresholding the GFRS response map and non-maximum suppression.

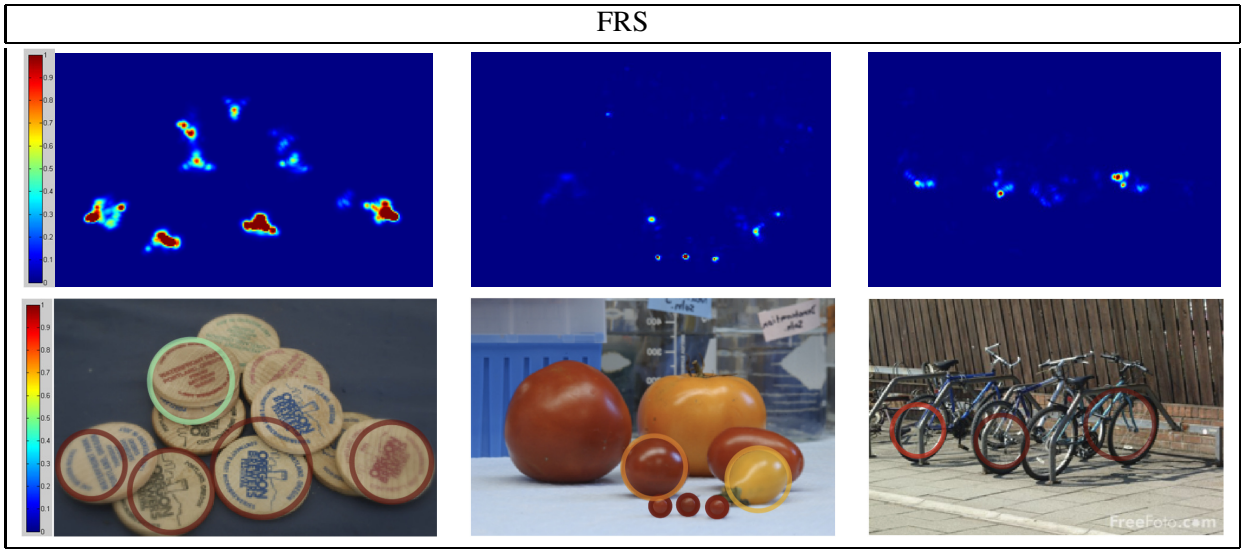

Figure 3. FRS applied to different real world images. Compared to Figure 2, many of the (elliptical) structures are not properly detected.

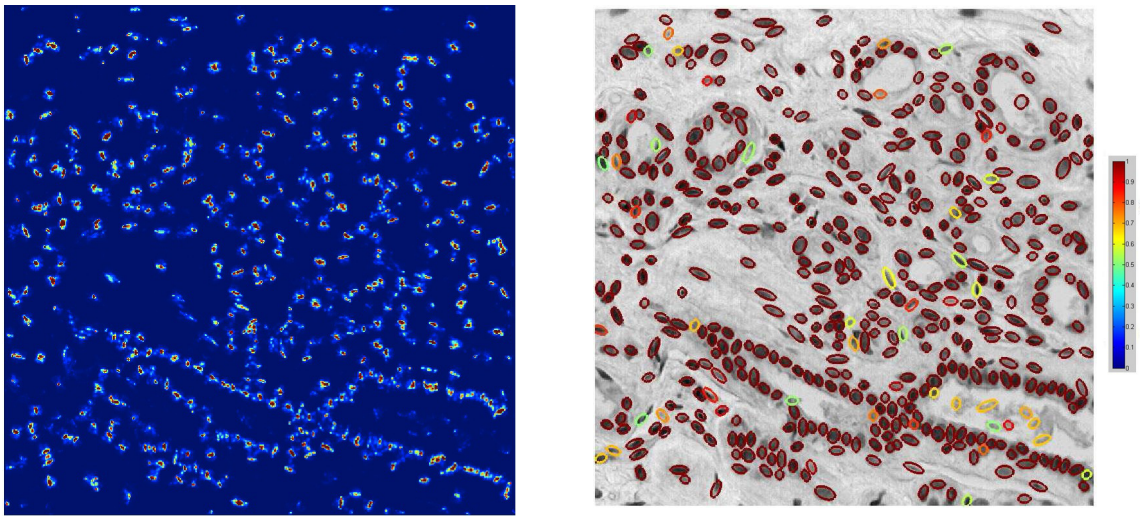

Figure 4. Nuclei detection of one histopathological image. Left: response map from GFRS; Right: detected nuclei.

4. Conclusions

In this paper, we have presented a novel and fast GFRS transform to detect radial symmetry in presence of (bounded) perspective transformations. We systematically extended the FRS transform for affine invariance while retaining linear complexity in image size. We also showed that it suffices to sample transformations from a (3d) subset of affine transformations (and not the larger space of perspective transformations). The wide applicability of GFRS to computer vision is demonstrated by applying it to a variety of everyday images. Further, we developed a GFRS nucleus detector for the important task of cell nuclei detection in biopsy samples from histopathology images. This is an important first step in automatic determination of presence and malignancy of cancer. The comparison between the GFRS nucleus detector and other state of the art detectors using ROC curves showed that GFRS achieves the best results reported to date.

Acknowledgement

We want to thank Andrei Chekkoury and Parmeshwar Khurd from Siemens Corporate Research for valu-

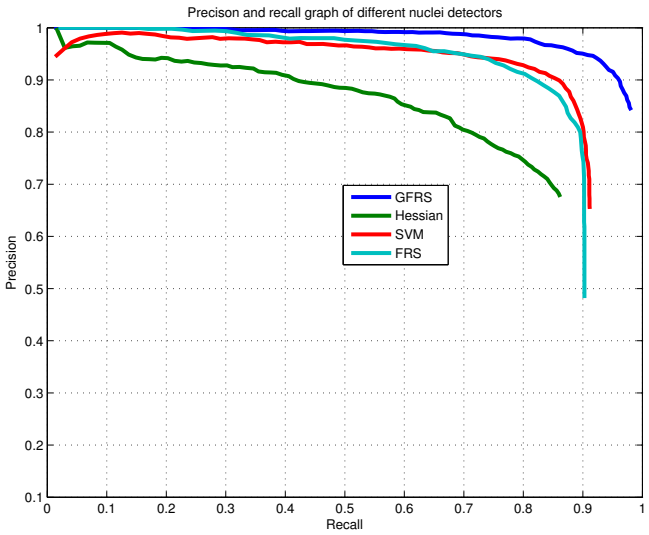

Figure 5. Precision and recall curve of nuclei detection from different methods. GFRS outperforms Hessian, SVM, and FRS based methods significantly.

able discussions and providing the code for the Hessian based nuclei detection. Part of this work was supported by National Institutes of Health/National Institute of Biomedical Imaging and Bioengineering (NIH/NIBIB) under Grant R01EB008055.

References

[1] G. Loy and A. Zelinsky, "Fast radial symmetry for detecting points of interest," *PAMI*, vol. 25, pp. 959–973, August 2003. 1, 2, 3, 4, 5

[2] K. Grammer and R. Thornhill, "Human (homo sapiens) facial attractiveness and sexual selection: The role of symmetry and averageness," *J. Comp. Psychol.*, vol. 108, pp. 233–242, 1994. 1

[3] G. Horridge, "The honeybee (apis mellifera) detects bilateral symmetry and discriminates its axis," *Journal of Insect Physiology*, vol. 42, pp. 755–764, 1996. 1

[4] H. Wilson and F. Wilkinson, "Symmetry perception: A novel approach for biological shapes," *Vision Research*, vol. 42, pp. 589–597, 2002. 1

[5] D. Reisfeld, H. Wolfson, and Y. Yeshurun, "Context free attentional operators: The generalized symmetry transform," *Intl J. Computer Vision*, vol. 14, pp. 119–130, 1995. 1

[6] S. Lee and Y. Liu, "Skewed rotation symmetry group detection," *PAMI*, vol. 32, no. 9, pp. 1659–1672, 2010. 1

[7] J. Maver, "Self-similarity and points of interest," *PAMI*, vol. 32, no. 7, pp. 1211–1226, 2010. 1

[8] H. Cornelius and G. Loy, "Detecting rotational symmetry under affine projection," in *ICPR*, 2006, pp. 292–295. 1, 2

[9] D. Ballard, "Generalizing the Hough transform to detect arbitrary shapes," *Pattern Recognition*, vol. 13, pp. 111–122, 1981. 1, 2

[10] T. Tuytelaars and K. Mikolajczyk, "Local invariant feature detectors: a survey," *Foundations and Trends in Computer Graphics and Vision*, vol. 3, no. 3, pp. 177–280, 2008. 2

[11] J. Matas, O. Chum, M. Urban, and T. Pajdlaa, "Robust wide-baseline stereo from maximally stable extremal regions," *Image and Vision Computing*, vol. 22, no. 10, pp. 761–767, 2004. 2

[12] Q. Yang and B. Parvin, "Perceptual organization of radial symmetries," in *In Proceedings, Computer Vision and Pattern Recognition*, 2004, pp. 320–325. 3

[13] R. Hartley and A. Zisserman, *Multiple View Geometry in Computer Vision*, 2nd ed. New York, NY, USA: Cambridge University Press, 2003. 3

[14] S. Maybank, "Application of the Fisher-Rao metric to ellipse detection," *Int. J. Comput. Vision*, vol. 72, pp. 287–307, May 2007. 3

[15] P. Khurd, L. Grady, A. Kamen, S. Gibbs-Strauss, E. Genega, and J. Frangioni, "Network cycle features: Application to computer-aided gleason grading of prostate cancer histopathological images," in *International Symposium on Biomedial Imaging*, 2011, pp. 1632–1636. 5

[16] C. Bilgin, P. Bullough, G. Plopper, and B. Yener, "Ecm-aware cell-graph mining for bone tissue modeling and classification," *Journal of Data Mining and Knowledge Discovery*, 2010. 5

[17] E. Cosatto, M. Miller, H. Graf, and J. Meyer, "Grading nuclear pleomorphism on histological micrographs," in *ICPR*, 2008, pp. 1–4. 5